Optics and Lasers in Engineering 139 (2021) 106503

Contents lists available at ScienceDirect

Optics and Lasers in Engineering

journal homepage: www.elsevier.com/locate/optlaseng

Scanning ion beam etching: A method for the fabrication of computer-generated hologram with nanometric accuracy for aspherical testing

Ruoqiu Wang[a], Zhiyu Zhang[a,*], Yingying Bai[a,b], Yanchao Wang[a], Xiaolin Yin[a,*], Lingsheng Kong[a], Weijie Deng[a], Donglin Xue[a], Xuejun Zhang[a]

[a] Key Laboratory of Optical System Advanced Manufacturing Technology of the Chinese Academy of Sciences, Changchun Institute of Optics, Fine Mechanics and Physics, Chinese Academy of Sciences, Changchun, Jilin 130033, China
[b] University of Chinese Academy of Sciences, Beijing 100049, China

ARTICLE INFO

Keywords:
Computer generated hologram
Ion beam etching
Optical testing

ABSTRACT

The phase type computer generated hologram (CGH) plays an important role in aspherical surface optical testing, especially for low reflectivity material mirror surfaces, owing to its high diffractive efficiency. With the increasing demand for high precision CGHs, traditional methods such as reactive ion etching and focusing ion beam, have difficulty realizing the fabrication of a large aperture and high accuracy phase type CGH. In this study, fabrication of a high precision CGH has been demonstrated via a new method called scanning ion beam etching (SIBE), which is suitable for most common optical materials and the fabrication of high performance CGH. On the basis of the movable radio frequency ion source, we determine an etching depth calculation method to realize high accuracy etching regardless of whether the removal function is a perfect Gaussian distribution. Experiments are conducted to verify the etching depth accuracy. Moreover, the linewidth, sidewall angle, roughness, and etching uniformity results of the CGH are superior to the fabrication of CGH via the conventional method. As a proof of concept, a phase type CGH with an aperture of 80 mm is fabricated, and the wavefront accuracy is 6.2 nm, which can meet the processing requirements of a high precision aspheric mirror. Thus, a SIBE method is developed for high performance CGH, which may aid in the development of high accuracy diffractive optics.

1. Introduction

Precision is one of the most important aspects of optical manufacturing. High precision creates high imaging quality, reliability, and added value for optical elements. In the past decades, remarkable advances have been achieved in the area of high-precision optical elements, where form accuracy is approaching the nanometer level, and surface roughness is approaching the atomic level.

Aspherical surfaces have been widely used in optical systems to provide improved imaging performances as well as reduced size and minimized weight. Form accuracy of aspherical surface is one of the most important factor to affect the imaging performance. For example, Our research team has produced a SiC aspherical mirror with a diameter of 4 m, a form accuracy of 18 nm RMS, and a surface roughness of 1 nm [1,2].

In recent years, diffractive optical elements (DOEs) have played an important role in the field of imaging systems [3], X-ray focusing [4], laser beam shaping [5], information storage [6], and optical system testing [7]. A computer generated hologram (CGH) is a special-designed DOE that can generate reference wavefronts of arbitrary aspherical surfaces. Therefore, it is a convenient and efficient "ruler" used in testing the form accuracy of aspherical lenses [8]. There is a saying that the highest accuracy of the aspherical surface depends on the precision of the CGH "ruler." However, it is very hard to fabricate a CGH to the nanometric level with surface roughness at the atomic level.

CGHs can be divided into amplitude and phase types. The former has chrome patterns on glass, while the latter has patterns etched into glass. Because the diffraction efficiency of a phase CGH is theoretically four times that of the amplitude type, it has obvious advantages in aspherical testing. Phase CGHs are usually fabricated by laser-direct lithography on a photoresist layer, followed by reaction ion etching (RIE) on fused silica substrate. The former step controls the horizontal positions of the CGH patterns, while the latter determines its vertical depth. It is proved that CGH patterns on a photoresist layer could be realized using high-precision laser-direct lithography. Nevertheless, it is difficult for RIE to simultaneously achieve both an accurate etching depth and a high

* Corresponding authors.
E-mail addresses: zhangzhiyu@ciomp.ac.cn (Z. Zhang), yinxiaolin1230@163.com (X. Yin).

https://doi.org/10.1016/j.optlaseng.2020.106503
Received 30 June 2020; Received in revised form 23 October 2020; Accepted 23 November 2020
Available online 7 December 2020
0143-8166/

Table 1
Comparison of different etching methods.

Etching methods	Principle	Advantange in CGH etching	Disadvantage in CGH ethcing
RIE	Chemical reaction &Physical sputtering	High etching rate	Worse etching roughness
ICP	Chemical reaction &Physical sputtering	High etching rate and accuracy	Limited processing range
FIB	Physical sputtering	Directly etching microstructure	Limited processing range&efficiency

uniformity when etching a large substrate. Generally, the depth uniformity achieved by commercial RIE equipment for a diameter of up to 100 mm is typically not better than 5%; hence, the wavefront accuracy of the RIE etched CGH is 13–17 nm in RMS, which could not be used directly in high-precision testing.

The etching depth error and substrate error of CGH can be canceled by subtracting the first-order measurement results from the zero-order results to achieve a CGH with an accuracy of 1 nm [9]. However, not all CGH can calibrated using this method, especially those designed for an off-axis aspherical mirror. In fact, this kind of aspherical mirror, with high steepness and large off-axis, relies heavily on CGH during optical manufacturing. Therefore, it is necessary to develop a high precision etching method to improve the wavefront accuracy of CGH.

Moreover, chemical reactions etching (RIE) process will worsen the roughness of the etched area [10,11]. Having a rough etching area is equivalent to introducing both amplitude error and etching depth error, which directly affects the accuracy of CGH [12,13]. Therefore, to achieve high precision phase CGH, the etching roughness should be rigorously restricted to being sub-nanometric [14,15]. In addition to the RIE method, inductively coupled plasma (ICP), and focusing ion beam (FIB) are common methods for DOE etching, but they have similar problems of limited processing range and low etching efficiency [16–18]. Table 1 summarizes the advantages and disadvantages of these etching methods for CGH fabrication.

To solve these problems, we develop a new method called scanning ion beam etching (SIBE) to simultaneously improve the etching depth uniformity and the surface roughness. SIBE is a physical etching method based on the movable inductively coupled radio frequency (RF) ion source, which can provide stable and pure plasma [19]. In this paper, first, we present an etching depth calculation method based on the imperfect Gaussian distribution of the ion source. Second, designed experiments are conducted to verify the etching performance by testing and analyzing all the characteristic parameters. Finally, a phase type CGH with an 80 mm aperture is fabricated. Nanometric accuracy wavefront and a sub-nanometric surface roughness are achieved. Therefore, the fabricated CGH could be directly used in high-precision aspherical testing. The results also indicate the feasibility and effectiveness of the SIBE method for etching DOE microstructures with extremely high precision.

In Section 2, the principle of the SIBE method is explained in detail. In Section 3, experiment are conducted to demonstrate the etching performance of SIBE. In Section 4, an 80 mm CGH is fabricated using the SIBE, the wavefront accuracy is tested and the error of this CGH are discussed.

2. Working principle of the SIBE

Since the 1970s, ion beam technology has been successfully applied to the correction and polishing of mirrors. High-energy, spatially distributed inert gas ions (mostly Ar ions) interact with atoms on the workpiece surface to achieve strictly controlled material removal, which can theoretically achieve atomic-scale removal [20,21].

In this work, we proposed to use a similar setup to achieve high-precision etching with the help of a photoresist mask with DOE patterns. As shown in Fig. 1, the ion beam source has a Gaussian-shape energy distribution, and its sputtering area radius is far less than the characteristic size of the diffracted element [22,23]. By scanning the Gaussian-shape source along a raster path, large-area etching could be easily achieved. Most importantly, the etching time T_i (also called dwell time) at each specified etching point along the scanning path is one of the variables in the algorithm of dwell time optimization, which could be utilized for improving the etching uniformity.

In addition, because the Gaussian-shape ion beam was originally used for the corrective polishing of aspherical and freeform surfaces [24], the etching of large-aperture CGHs via this method enables the simultaneous etching and corrective polishing of the treated substrate.

Moreover, the SIBE can be used to remove materials with almost no restriction on the material type, which fundamentally determines that SIBE can be used for etching of most kinds of optical materials such as silica, fused silica, zerodur, aluminum, chromium, and so on.

To account for the low denaturation temperature (145 ˚C) of the photoresist mask, a low ion energy and current should be adopted during etching process. Owing to this restriction, the shape of the removal function will usually have a relatively large deviation with a Gaussian type, which can incur a large residual error after Gaussian fitting, thus affecting etching accuracy. According to the traditional deconvolution method [25],

$$h(x, y) = R(x, y) ** T(x, y) \tag{1}$$

where $h(x, y)$ is the calculated etching depth distribution, R(x, y) is the removal function distribution, and $T(x, y)$ is dwell time distribution of the ion beam during the etching process. To obtain a mean etching depth distribution $h(x, y)$ or actually h_0, the $T(x, y)$ must also be a mean distribution t_0. The h_0 is always proportional to the t_0 regardless of the distribution of the removal function.

According to this principle, we present a new concept called “SIBE velocity” to describe the etching process. As shown in Fig. 1, the velocity is related to the scanning step distance d, dwell time of single point t, and etching parameters of SIBE. Generally, once the parameters are confirmed, they will not change. Through the first calibration experiment, the relationship between etching depth h_0 and the velocity parameter can be expressed as

$$v = h_0 d_0^2 / t_0 \tag{2}$$

To acquire the anticipated etching depth h_1, the dwell time distribution t_1 can be calculated through the velocity after the stepping distance is confirmed, as follows:

$$\begin{aligned} t_1 &= h_1 d_1^2 / v \\ &= h_1 d_1^2 t_0 / h_0 d_0^2 \end{aligned} \tag{3}$$

Based on the dwell time calibration experiments, the designed etching depth can be accomplished with high accuracy regardless of whether the removal function is perfect Gaussian distribution.

To verify the stability and accuracy of the RF ion source, a stability experiment was carried out under a set of fixed parameters for the ion beam processing of fused silica as shown in Table 2. In the 8 h time span, single point dwell processing was performed 10 times for 100 s each, and the processing result is shown in Fig. 2.

The characteristic value of the removal function of each point can be obtained by Gaussian fitting. The RMS value of fitting residual error is smaller than 2 nm. The error of characteristic values is given in Table 3, which shows the stability of removal functions.

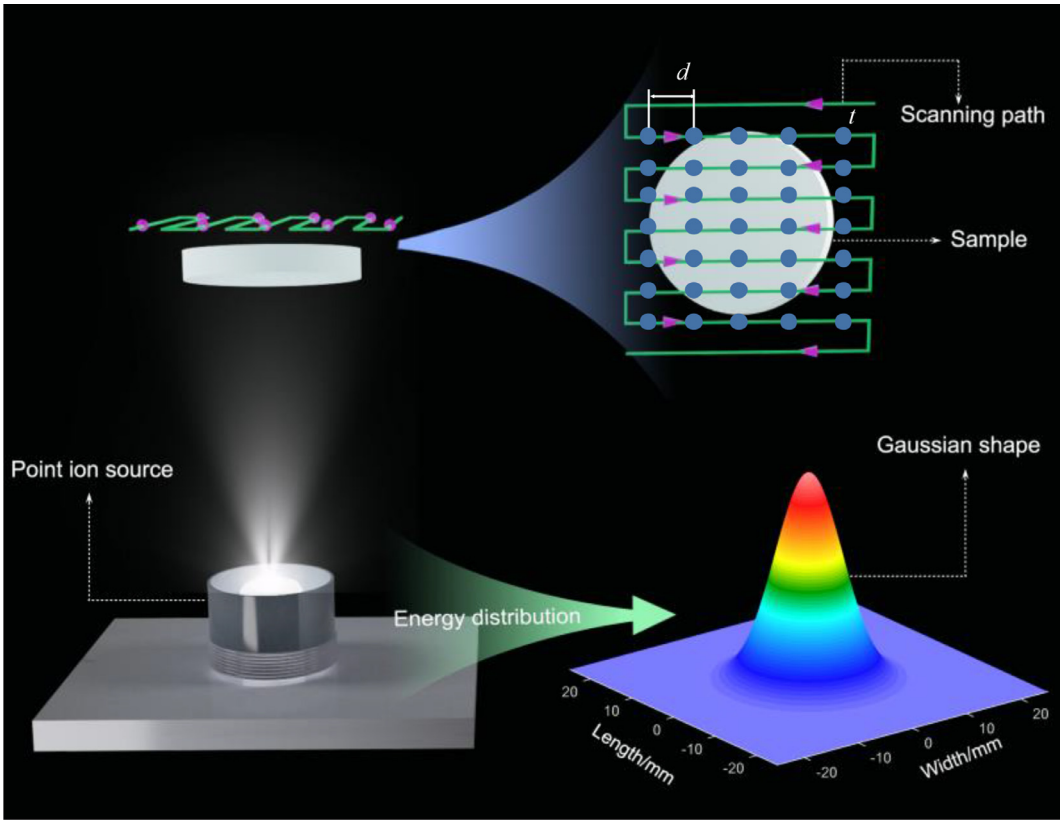

Fig. 1. Schematic of the SIBE process.

Table 2
Parameters of ion source for stability testing experiment.

Item	Ion Energy (eV)	Beam Current (mA)	Grid Size (mm)	Neutralization (mA)	Etching Time (s)	Distance (mm)
Value	1000	1.5	10	50	100	30

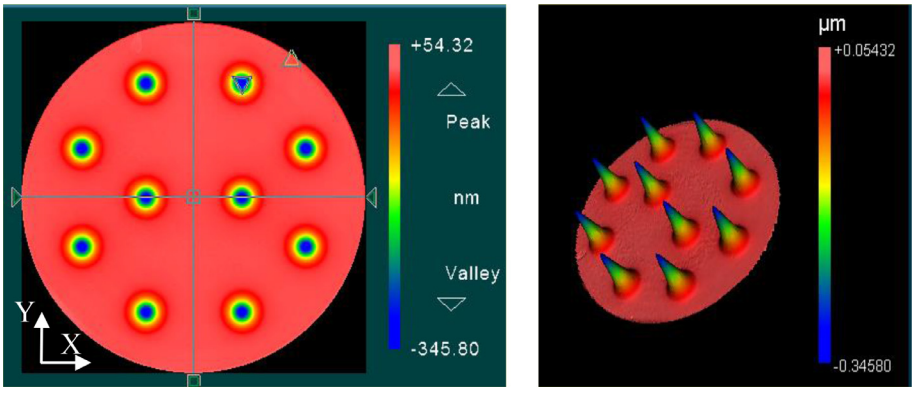

Fig. 2. Processing result of the stability experiment.

Table 3
Stability results of removal functions (PV Error).

Item	Etching Rate	FWHM X	FWHM Y	Volume Etching Rate
Value	3.127%	0.947%	0.965%	2.894%

3. SIBE experiments

To verify the etching performance of the SIBE method, etching structures with common stripe lines of CGH from 3 to 100 micrometers with a 0.5 duty cycle were designed to conduct the experiments. Considering the properties of photoresist mask will be affected by the temperature change, the etching process was divided into several segments to reduce the thermal effect [26]. The parameters of the ion source are shown in Table 4. For each instance of the etching process, the scanning step distance d is 0.5 mm and the dwell time of single point t is 20 ms. The four fused silica substrates with designed structures are etched from 1 to 4 times.

After SIBE, the stripe profiles of the four test substrates were tested, and the results are shown in Fig. 3. Fig. 3(c) shows the test results for etching depth. The abscissa represents the measured width of the

Table 4
Parameters of the ion source for etching experiment.

Item	Ion Energy (eV)	Beam Current (mA)	Grid Size (mm)	Neutralization (mA)	Distance (mm)
Value	700	22	37	80	80

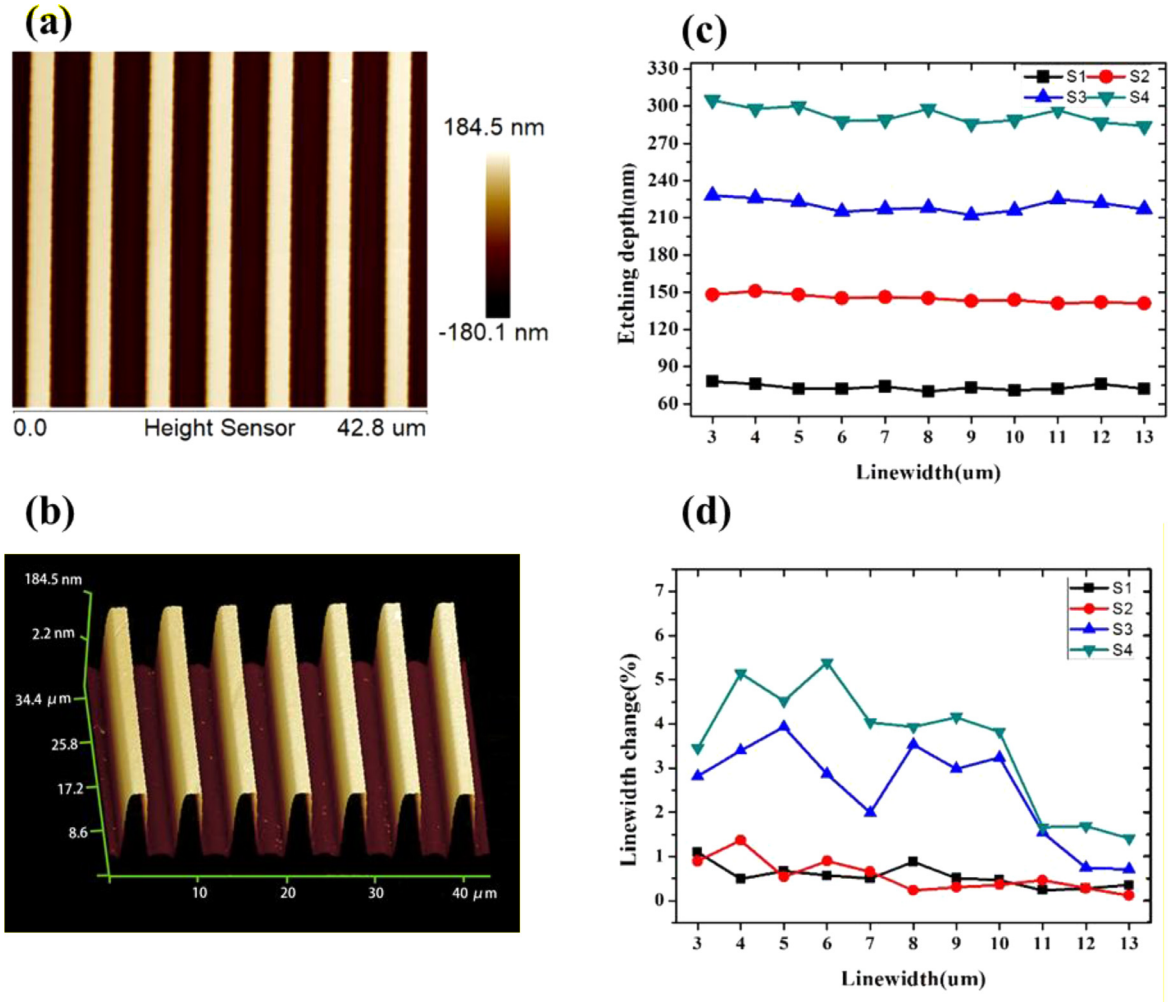

Fig. 3. Test results of four test substrate. (a) Stripe profile as tested by AFM; (b) Three-dimensional profile of etching stripes; (c) Etching depth test results; (d) Linewidth change test results.

line while the ordinate represents the measured depth. The mean values of the four test substrates are 73.3 nm, 144.9 nm, 219.9 nm, and 292.8 nm, showing a good linear relationship between etching depth and etching time. The standard deviation of etching depth is calculated as $\sigma_1 = 2.453$ nm, $\sigma_2 = 3.177$ nm, $\sigma_3 = 5.147$ nm, and $\sigma_4 = 6.940$ nm. It can be observed that with the increase in etching depth, the uniformity fluctuates slightly but is still less than 7 nm. The width of the line would not affect the etching depth or the uniformity. The measurement results will be used as input parameters for the etching process to guide the fabrication of CGH.

Although SIBE belongs to anisotropic etching, which can effectively avoid linewidth broadening, because the lithographic exposure forms a trapezoidal structure on the photoresist, the thin bottom angle will be consumed first and the substrate etching will then cause the linewidth to broaden. Fig. 3(d) gives test results of linewidth change. The linewidth broaden with the etching number and the etching depth increase, the linewidth change is related to the etching depth h and the angle θ of the trapezoidal photoresist, which can be expressed as

$$l = \frac{2h}{\tan\theta} \tag{4}$$

The test substrate achieved the angle of 65°, and the test results showed that the substrates S1 and S2 hold the linewidth change within 1.5%, whereas the linewidth broadening of S3 and S4 increased obviously along with the etching depth and number to larger than 3%, which could not be accepted. The linewidth change caused by SIBE was much smaller than that with the isotropic etching method, and this change can also be compensated during the photolithograph. The sidewall angle after etching is about 50°, which is far better than RIE.

The roughness test results for the top and bottom area of the stripes are shown in Fig. 4(a) and (b), and both have Ra values of 0.4 nm. Because the SIBE belongs to physical removal, the roughness of the etched area (bottom of stripes) will not change, and may even be homogenized. Because SIBE shows excellent performance in etching roughness, it has great advantages in the fabrication of high precision phase CGH.

4. Fabrication of the CGH

To investigate the performance of SIBE in the fabrication of a CGH, we designed and fabricated a phase CGH with a diameter of 80 mm. The designed CGH pattern was firstly exposed on a photoresist layer

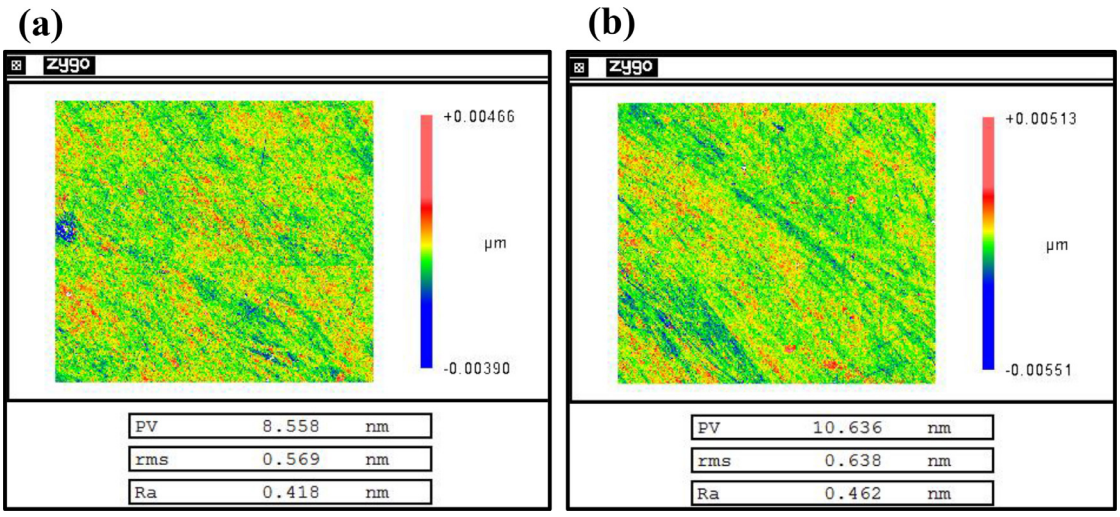

Fig. 4. Roughness test results of different area. (a) unetched area; (b) etched area.

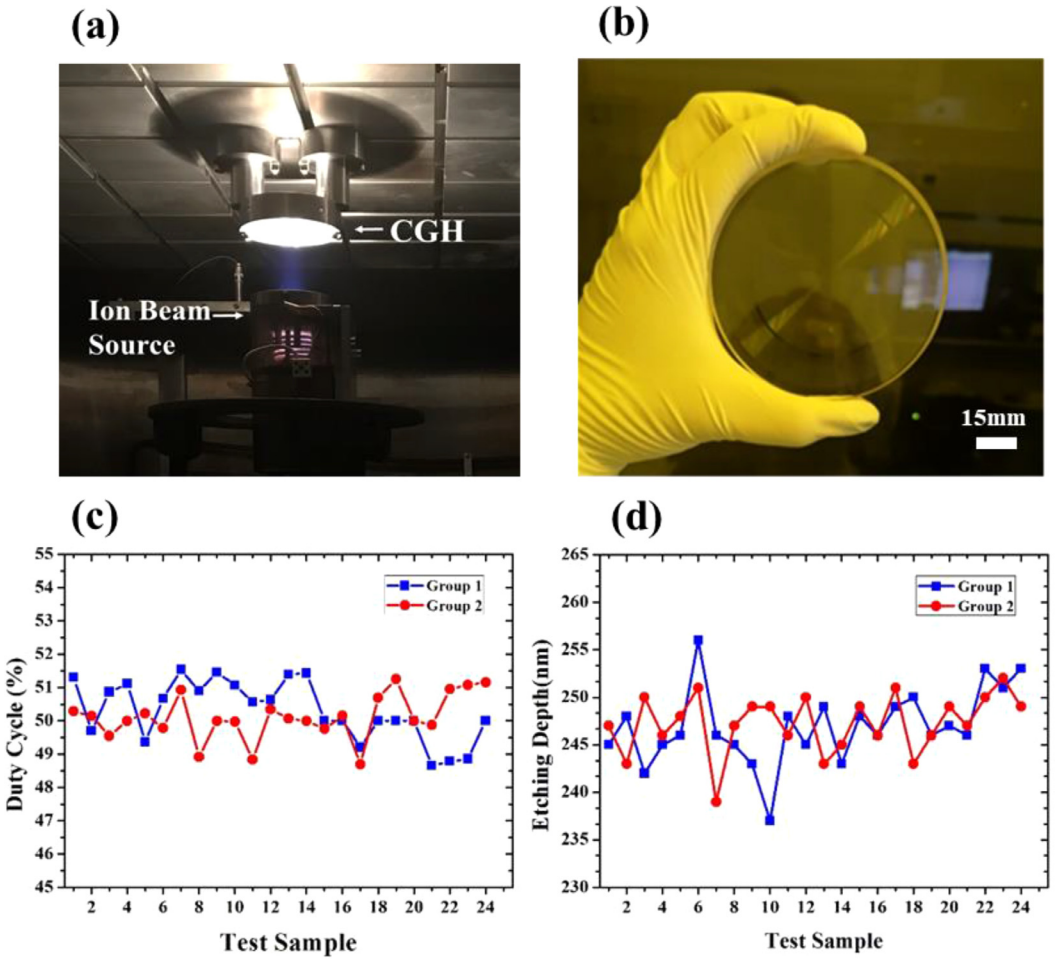

Fig. 5. Profile test results of phase CGH with a diameter of 80 mm; (a) The etching process in SIBE; (b) Phase CGH after etching; (c) Duty cycle test results with a sampling interval of 2 mm; (d) Etching depth test results with a sampling interval of 2 mm.

by laser direct writing (DWL4000, Heidelberg Instruments, Germany). After development and hardbaking, the physical etching process is performed using SIBE equipment as shown in Fig. 5(a), and Fig. 5(b) shows a photo of the phase CGH.

Along the radial direction of the CGH, the cross-section profile was measured at a sampling interval of 2 mm. The linewidth of sampling points changed from 50 μm at the center to 1.8 μm at the margin. As shown in Fig. 5, the mean square deviation of etching depth in the full aperture range is 3.5 nm, and the etching depth uniformity is less than 1.5%.

Next, the wavefront accuracy of the fabricated CGH was tested. Fig. 6(a) showed the light path of the CGH wavefront accuracy test. A

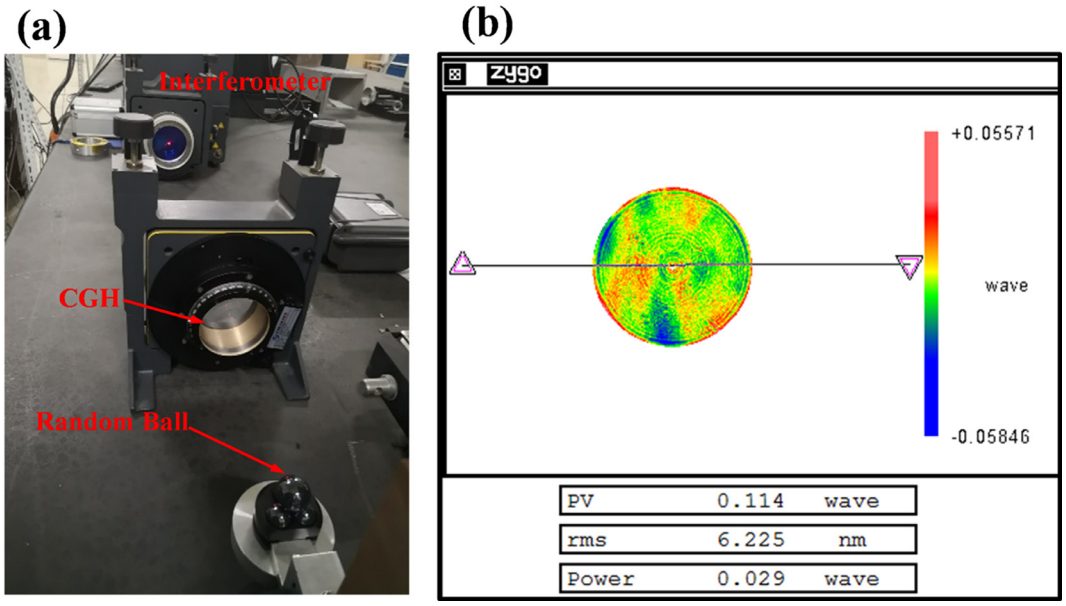

Fig. 6. (a) Light path of CGH's wavefront accuracy test; (b) Wavefront test result of CGH test area.

calibration ball was used as the CGH's test surface. After passing through the CGH, the divergent spherical waves emitted by interferometer were transformed into convergent spherical waves. The +1 diffractive light is converged in the center of the calibration ball.

The interferometer is a Zygo Verifire PE (wavelength = 632.8 nm), and the size of the reference lens is 4 inches, F# = 3.3. The calibration ball has a diameter of 20 mm and an accuracy of 0.6 nm, which is far higher than the CGH accuracy. During the test, first, the CGH was aligned with the interferometer using the alignment area of the CGH, and then the position of the calibration ball was adjusted to achieve zero fringe in the test area. The test result is shown in Fig. 6(b). The wavefront accuracy was 6.2 nm, which can fully meet the requirements of high precision optical lens.

5. Conclusions

In this study, we develop the SIBE method, a novel etching method to achieve a phase CGH with nanometric precision. The SIBE velocity was proposed to achieve accurate etching depth through calculation and calibration. A phase CGH with an aperture of 80 mm is fabricated using SIBE and achieves etching uniformity better than 1.5%. The etching area has the same roughness of 0.4 nm with the unetched area. The wavefront accuracy is 6.2 nm, which can meet the processing requirements of a high precision aspheric mirror. It can be proved that the SIBE is an effective method for the etching of high precision micro-nano structures. In this study the SIBE method shows good performance in microstructure etching, SIBE can also be used to fabricate large substrates with a possible maximum aperture of 1500 mm. This potential is of great importance for improving the fabrication precision of larger-aperture FZP, especially in the building of next-generation giant space telescopes. One existing problem now is the low etching rate. Although the etching rate can be increased by increasing the ion energy, the heat accumulation of high ion energy will lead to the denaturation of the photoresist mask, thus reducing the etching accuracy. Our future work will focus on the thermal effect control to improve the etching efficiency.

Funding

This work was supported by the Advanced Science Key Research Project, Chinese Academy of Science (QYZDJ-SSW-JSC038), and Key Foreign Cooperation Projects of International Cooperation Bureau, Chinese Academy of Science (181722KYSB20180015). This work was partially supported by the National Nature Science Foundation of China (51775531, 11903036 and 61705221).

Declaration of Competing Interest

The authors declare that they have no known competing financial interests or personal relationships that could have appeared to influence the work reported in this paper.

Supplementary materials

Supplementary material associated with this article can be found, in the online version, at doi:10.1016/j.optlaseng.2020.106503.

CRediT authorship contribution statement

Ruoqiu Wang: Conceptualization, Investigation, Methodology, Writing - original draft. **Zhiyu Zhang:** Supervision, Funding acquisition, Writing - review & editing. **Yingying Bai:** Investigation, Software, Data curation. **Yanchao Wang:** Formal analysis, Visualization. **Xiaolin Yin:** Supervision, Writing - review & editing. **Lingsheng Kong:** Resources, Funding acquisition. **Weijie Deng:** Resources, Project administration. **Donglin Xue:** Supervision, Software. **Xuejun Zhang:** Resources, Funding acquisition.

References

[1] Ge Z, Congcong C, Binchao D, Qi C, Jianxun B. Fabricating of Φ4m CIOMP-SiC mirror blank. Proc SPIE 2019;10837:108370I. doi:10.1117/12.2505588.
[2] Yang B, Longxiang L, Donglin X, et al. Rapid fabrication of a silicon modification layer on silicon carbide substrate. Appl Opt 2016;55(22):5814–20. doi:10.1364/AO.55.005814.
[3] Wang P, Mohammed N, Shen B, et al. Broadband imaging with one planar diffractive lens. Sci Rep 2018;8:1−;6 2799. doi:10.1038/s41598-018-21169-4.
[4] Sasa B, Mauro P, Holger F, et al. X-ray focusing with efficient high-NA multilayer Laue lenses. Light Sci Appl 2018;7(3):1–9 17162. doi:10.1038/lsa.2017.162.
[5] Qu W, Gu H, Tan AQ. Design of refractive/diffractive hybrid optical elements for beam shaping with large diffraction pattern. Chin Opt Lett 2016;14(3):031404. doi:10.3788/COL201614.031404.
[6] Lin SIE. Study and implementation of a hybrid diffractive/refractive lens and a color inkjet head on high density data storage. Appl Opt 2011;50(8):1091–100. doi:10.1364/AO.50.001091.
[7] Feng W, Zhiyu Z, Ruoqiu W, Xuefeng Z, et al. Distortion measurement of optical system using phase diffractive beam splitter. Opt Express 2019;27(21):29803–16. doi:10.1364/OE.27.029803.

[8] Malacara D. Optical shop testing. 3rd ed. New Jersey: John Wiley & Sons; 2007. 2007.
[9] Ping Z, James B. Fabrication error analysis and experimental demonstration for computer-generated holograms. Appl Opt 2007;46:657–63. doi:10.1364/AO.46.000657.
[10] Andrzej K, Zbigniew J, Krzysztof G. Diffractive optical elements obtained using electron-beam writer and reactive ion etching. Microelectron Eng 2002;4887:141–147. doi:10.1117/12.475983.
[11] Seiji N, Sumio N, Shoso S, et al. Fabrication of the multi-level phase type hologram for display using the laser direct write lithography system. Proc SPIE 2012;8281 828116-1–6. doi:10.1117/12.909826.
[12] Ping Z, James H B. Optimal design of computer-generated holograms to minimize sensitivity to fabrication errors. Opt Express 2017;15(23):15410–17. doi:10.1364/OE.15.015410.
[13] Ping Z, James B. Coupling of surface roughness to the performance of computer-generated holograms. Appl Opt 2007;46:6572–6. doi:10.1364/AO.46.006572.
[14] Curatu E, Wang M. Tolerancing and testing of CGH aspheric nulls. Proc SPIE 1999;3782:581–99. doi:10.1117/12.369208.
[15] Yuchun C, Ping Z, James B. Analysis of phase sensitivity for binary computer-generated holograms. Appl Opt 2006(45):4223–34. doi:10.1364/AO.45.004223.
[16] Tan X, Jiao Q B, Qi X D, Bayan H. Fabrication of high-efficiency and low-stray–light grating by inductively coupled plasma (ICP) etching-polishing method. Opt Express 2016;24(6):5896–910. doi:10.1364/OE.24.005896.
[17] Kim H B, Hobler G, Steiger A, et al. Simulation-based approach for the accurate fabrication of blazed grating structures by FIB. Opt Express 2007;15(15):9444–9. doi:10.1364/OE.15.009444.
[18] Janeiro R, Flores R, Dahal P, et al. Fabrication of a phase photon sieve on an optical fiber tip by focused ion beam nanomachining for improved fiber to silicon photonics waveguide light coupling. Opt Express 2016;24(11):11611. doi:10.1364/OE.24.011611.
[19] Ying L, Xuhui X, Lin Z, Zuocai D, Guiyang C. Improve optics fabrication efficiency by using a radio frequency ion beam figuring tool. Appl Opt 2017;56(2):260–6. doi:10.1364/AO.56.000260.
[20] Allen LN, Roming HW. Demonstration of an ion figuring process. Proc SPIE 1990;1333:22–33. doi:10.1117/12.22383.
[21] Allen LN, Hannon JJ, Wambach RW. Final surface error correction of an off-axis aspheric petal by ion figuring. Proc SPIE 1991;1543:190–200. doi:10.1117/12.51181.
[22] Tang W, Deng W, Yin X, et al. Computation of the removal function for ion beam figuring curved surface. J Comput Theor Nanos 2016;13(10):7025–31. doi:10.1166/jctn.2016.5664.
[23] Malobabic S, Jupé M, Ristau D. Spatial separation effects in a guiding procedure in a modified ion-beam-sputtering process. Light Sci Appl 2015;5(3). doi:10.1007/978-3-540-76694-0_148.
[24] Sigmund P. Theory of sputtering. I. Sputtering yield of amorphous and polycrystalline targets. Phys Rev 1969;184(2):383–416. doi:10.1103/PhysRev.187.768.
[25] Wu J F, Lu Z W, Zhang H X, et al. Dwell time algorithm in ion beam figuring. Appl Opt 2009;48(20):3930–7. doi:10.1364/AO.48.003930.
[26] Xiaolin Y, Weijie D, Wa T, Binzhi Z, Xuejun Z. Ion beam figuring approach for thermally sensitive space optics. Appl Opt 2016;55(28):8049–55. doi:10.1364/AO.55.008049.